

Article.

Reinforcement of Alginate-Gelatin hydrogels with Bioceramics for biomedical applications: a comparative study

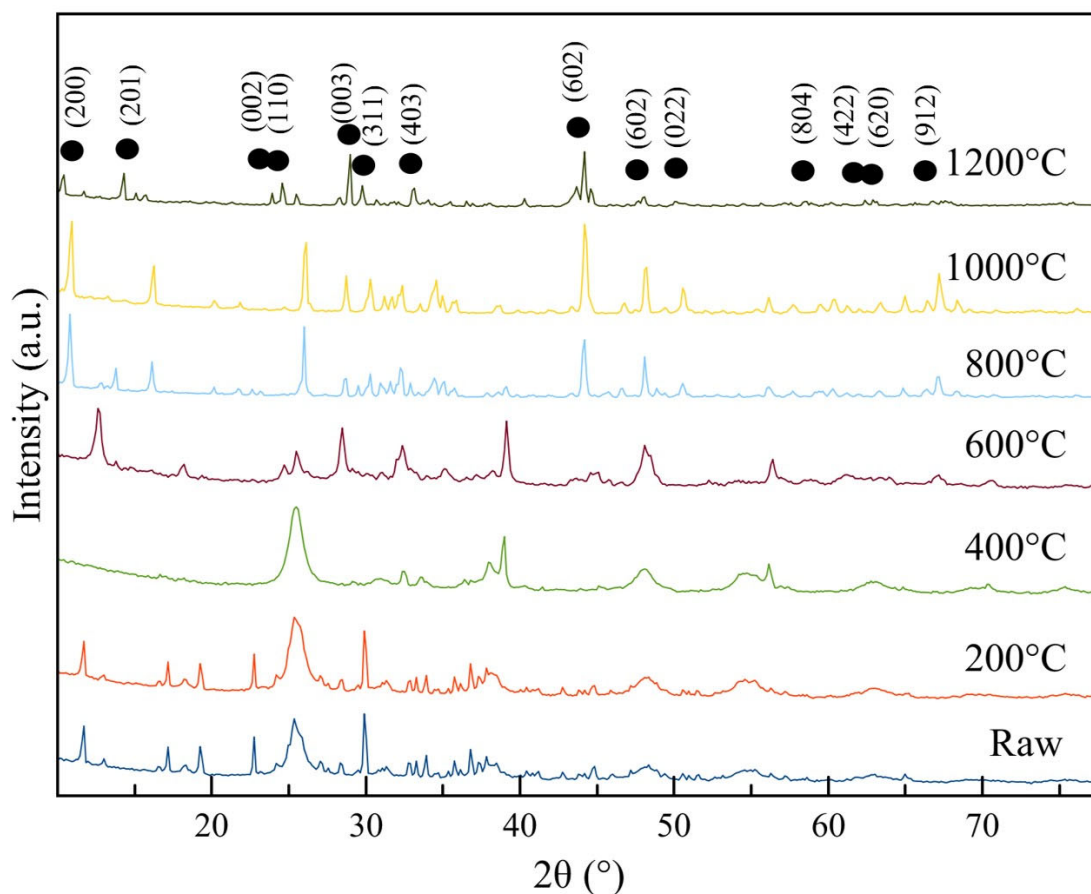
Alan Avila-Ramirez^{1,2}, Kevin Katzim-Rios¹, Carlos Enrique Guerrero-Beltrán³, Erick Ramírez-Cedillo¹, Wendy Ortega-Lara^{1,*}

¹ Tecnológico de Monterrey; Escuela de Ingeniería y Ciencias

² Division of Biological & Environmental Science & Engineering (BESE), King Abdullah University of Science and Technology (KAUST), Thuwal 23955-6900, Saudi Arabia

³ Tecnológico de Monterrey, Escuela de Medicina y Ciencias de la Salud, Medicina Cardiovascular y Metabólica, Monterrey, N.L. México; enriqueguerrero@tec.mx

* Correspondence: wlortega@tec.mx;



$\text{Na}_2\text{Ti}_6\text{O}_{13}$

Figure S1. X-ray diffractogram of $\text{Na}_2\text{Ti}_6\text{O}_{13}$ synthesis with different temperatures of calcination until 1200°C

The pronounced peaks of figure S1 indicate the XRD patterns of the samples synthesized from sodium acetate and titanium butoxide (IV), which are indexed to $\text{Na}_2\text{Ti}_6\text{O}_{13}$ phase (monoclinic structure) space group. Prominent peaks belong to Anatase (TiO_2) in lower temperatures, indicating the starting materials have been almost turning into $\text{Na}_2\text{Ti}_6\text{O}_{13}$ products at 1200°C . At lower temperatures below 1000°C it can be seen different peaks corresponding to Anatase (TiO_2), which peaks crystal structure (2theta) at 25° , 39° and 47° , obtained from ISCD (01-071-1168), and Rutile (TiO_2) since 600° with 27° , 48° and 56° , before the desired crystal at the 1200°C of calcination(1) (2).

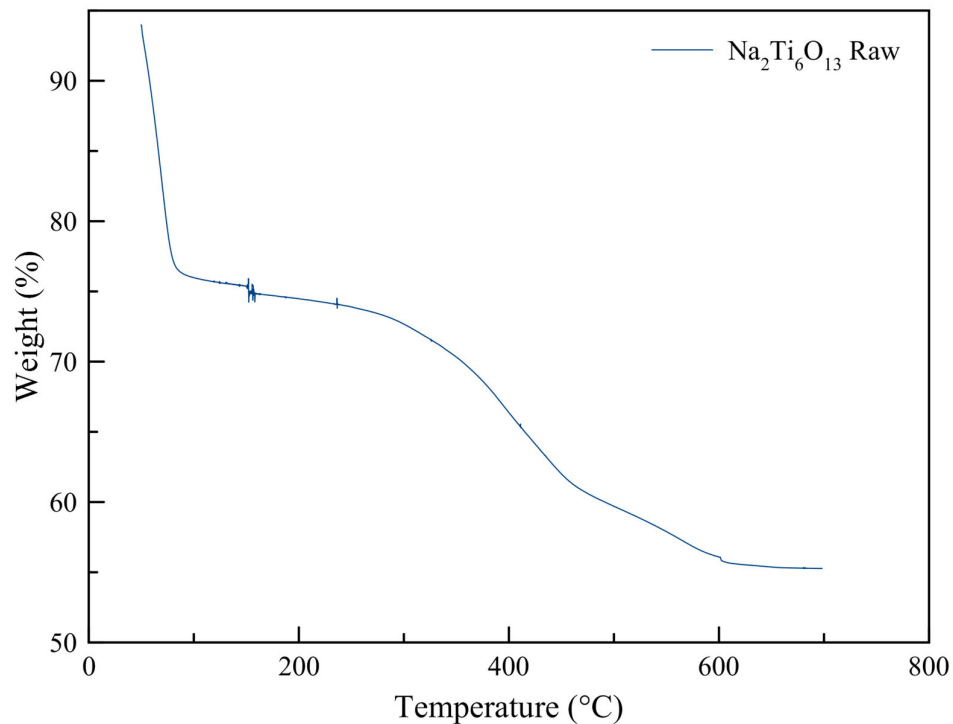


Figure S2. Thermogravimetric analysis spectra from pre-calcined $\text{Na}_2\text{Ti}_6\text{O}_{13}$

The evolution of gravimetric loss is elucidated in the range from around 90°C to 150°C the last of 25% of weight due to the loss of water and hydroxyl groups that are coordinated to the initial pre-calcined samples due to solvents as tert-butanol, deionized water, and coordinated water bonds from sodium acetate that are used in thermal synthesis step before calcination at high temperatures. A second weight-loss of 30% from 250°C to 600°C represents the loss of carbonyl from sodium acetate and by the rearrangements and loss of oxygen atoms until getting the desired structure (3).

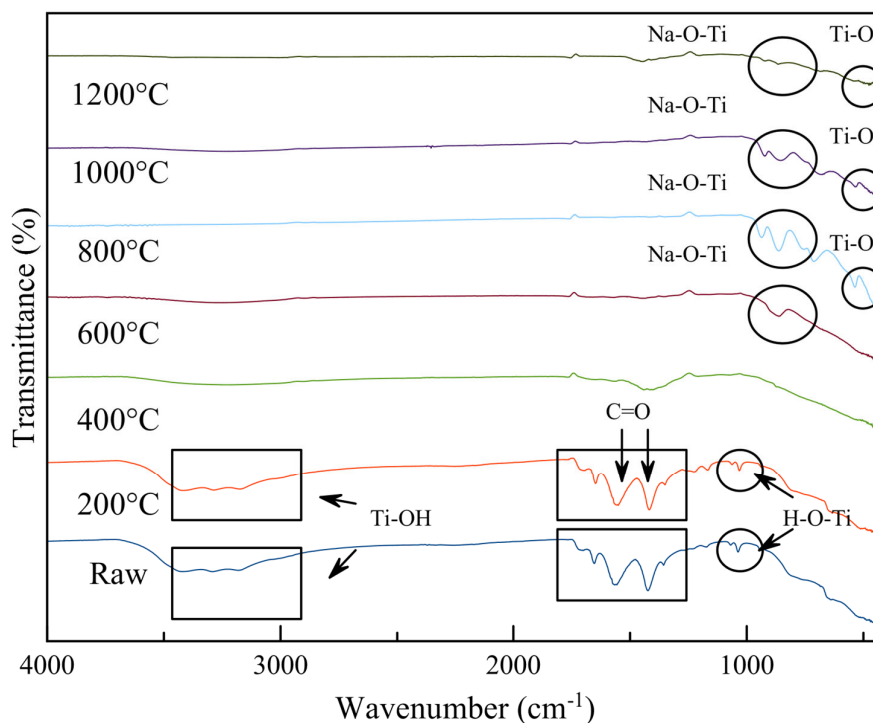


Figure S3. FT-IR spectra from pre-calcined raw $\text{Na}_2\text{Ti}_6\text{O}_{13}$ material to calcined higher temperatures

FT-IR studies from figure S5 show that the bands at 1730 cm^{-1} and 3150 cm^{-1} are related to the bending and stretching modes of the chemisorbed or interlamellar water molecules. It is essential to mention that the shoulder at 2900 cm^{-1} belongs to the interaction between Ti-OH ions at temperatures below $400\text{ }^\circ\text{C}$. When the temperature increases in post-synthesis, that the signal from water was removed, and the Ti-OH bonds were modified. Sodium titanates contain Ti-O and Ti-OH is stretching and bending vibration bands with different intensities in the region $500\text{--}1000\text{ cm}^{-1}$. The peak at 910 cm^{-1} corresponds to Na-O-Ti, and bonds in TiO_6 octahedra appear at $600\text{ }^\circ\text{C}$ and above this temperature. The small peak at 974 cm^{-1} is due to the bending vibrations of Ti-OH non-bridging bonds in the as-made sample. The alkali-oxygen vibrations usually provide absorption bands at 1440 , 1370 , 1060 , and 880 cm^{-1} . The short peaks near 500 cm^{-1} correspond to Ti-O when achieving calcination up to $600\text{ }^\circ\text{C}$ or higher temperatures until $1200\text{ }^\circ\text{C}$. The sharp peak at 1460 cm^{-1} of the dehydrated sample is attributable to new alkali-oxygen (Na-O). The low-intensity broadband in the $3200\text{--}3600\text{ cm}^{-1}$ region and the band centered at 1625 cm^{-1} are assigned to O-H stretching and deformation vibrations of weakly bound water, giving evidence for the existence of Ti-OH or Ti=O groups due to Titanium(IV) butoxide, that was used in the synthesis protocol as the precursor of titanium ions meanwhile the two bands with high intensity at raw, and $200\text{ }^\circ\text{C}$ correspond to carbonyl groups which are from the sodium acetate that disappear at higher temperatures. Peaks corresponding to the bending vibrations of the Ti-O groups at 506 and 448 cm^{-1} converge into a broader peak centered at around 480 cm^{-1} seen from $800\text{ }^\circ\text{C}$ to $1200\text{ }^\circ\text{C}$; this by the elimination of hydration and the rearrangement of atoms. The shoulder at 878 cm^{-1} is characteristic of the Na-O bending of the Na-O-Ti bond of sodium titanates, whereas the minimal signal at 1061 cm^{-1} can be attributed to the respective bending vibration H-O-Ti of the hydroxyl titanates (4, 5), (6), (7).

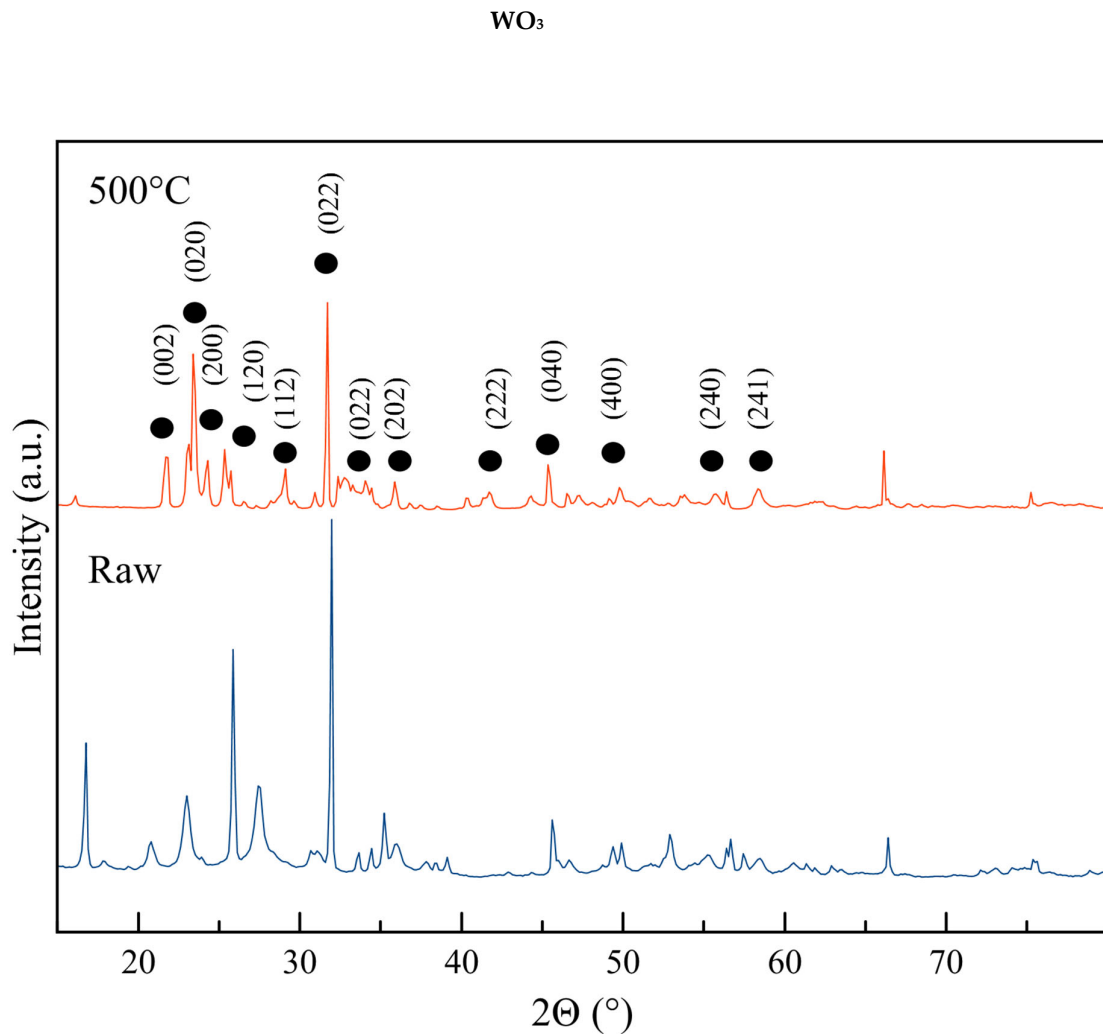


Figure S4. X-ray diffraction from the synthesis of raw pre-calcined and 500°C calcination of WO_3

From the XRD pattern of Fig S2, WO_3 particles calcined at 500°C are monoclinic crystals has their highest (022) peak was at 34° with low intensity of (020) at peak 23° peak, while a peak with increased intensity of WO_3 (200) at 24° . The previous information is obtained from ICSD (00-024-0747). WO_3 showed balanced peak intensity among all three samples, indicating the crystal's presence (8), (9). In the case of the structure of the raw pre-calcinate material showing residues of NaWO_3 dehydrated, that is presented in the 2θ at 16° and 27° (10).

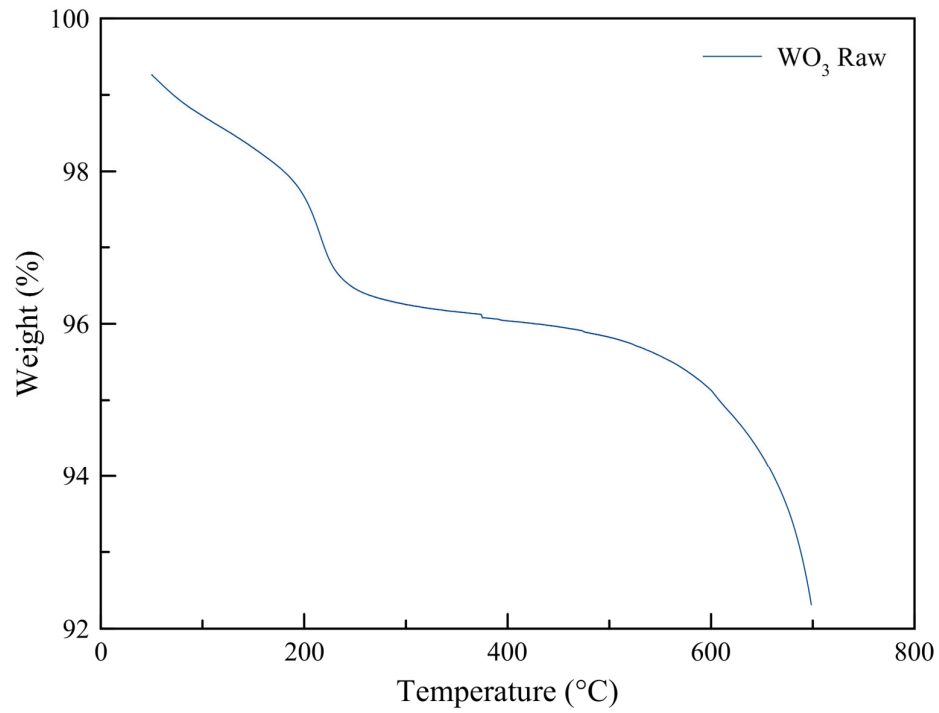


Figure S5. Thermogravimetric analysis spectra from pre-calcined WO₃

In the thermogravimetric analysis from figure S4 of WO₃, before 200°C the decay of the slope corresponds to the elimination of the coordinated water molecules attached initially by the sodium tungstate dihydrate precursor. There is a constant behavior until the degradation at 600°C. Therefore, while synthesizing the particles at 500°C, the final structure does not lose a significant percentage of weight from 200°C to 600°C (11).

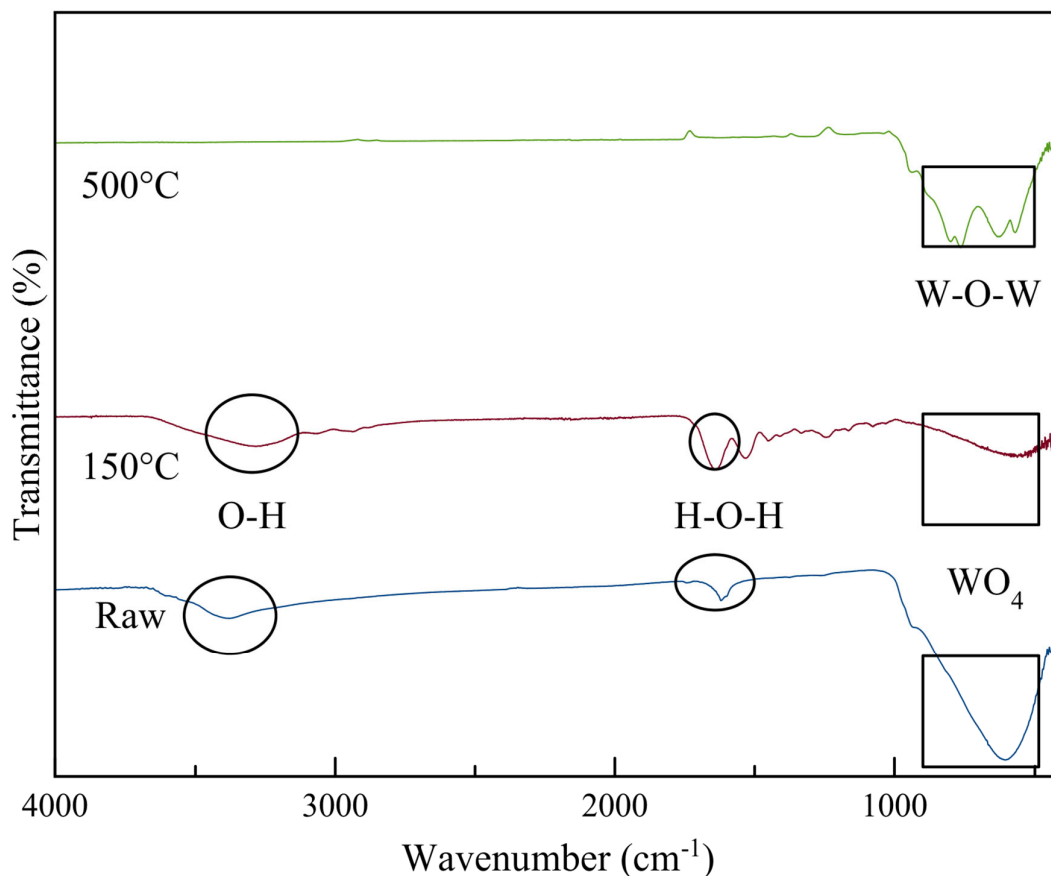


Figure S6. FT-IR from WO_3 pre-calcined and with different temperatures of calcination

The higher bands at the $3700\text{--}3100\text{ cm}^{-1}$ region are observed due to OH groups and adsorbed water. Specifically, the broad bands at 3450 and 3692 cm^{-1} are due to various O–H stretching modes and a sharp mode at 1620 cm^{-1} is the H–O–H bending mode. Conversely, no bands were observed in the region $3400\text{--}3700\text{ cm}^{-1}$ or at 1620 cm^{-1} when calcined at higher temperatures. The shallow or superficial shoulder, located around 600 cm^{-1} in the pre-calcined powders, can refer to the initial WO_4 from the tungstate precursor. The W–O peak shifts towards higher wavenumbers, at 813 cm^{-1} , where this shift corresponds to the formation of W–O–W crystalline bonds that gives information about the changes, from raw to calcined powders 500°C (12) (13).

References

1. Luo, L., Zhen, Y., Lu, Y., Zhou, K., Huang, J., Huang, Z., Mathur, S., and Hong, Z. (2020) Structural evolution from layered $\text{Na}_2\text{Ti}_3\text{O}_7$ to $\text{Na}_2\text{Ti}_6\text{O}_{13}$ nanowires enabling a highly reversible anode for Mg-ion batteries, *Nanoscale*.
2. (2018) Titanium butoxide molar ratio effect in the TiO_2 nanoparticles size and methylene blue degradation, *Optik*, Urban & Fischer 157, 890–894.
3. Torres-Martínez, L. M., Juárez-Ramírez, I., Del Ángel-Sánchez, K., Garza-Tovar, L., Cruz-López, A., and Del Ángel, G. (2008) Rietveld refinement of sol-gel $\text{Na}_2\text{Ti}_6\text{O}_{13}$ and its photocatalytic performance on the degradation of methylene blue, *Journal of Sol-Gel Science and Technology*.
4. Shirpour, M., Cabana, J., and Doeff, M. (2013) New materials based on a layered sodium titanate for dual electrochemical Na and Li intercalation systems, *Energy Environ. Sci.*, The Royal Society of Chemistry 6, 2538–2547.
5. Jian, Z., Huang, S., and Zhang, Y. (2013) Photocatalytic Degradation of 2,4-Dichlorophenol Using Nanosized $\text{Na}_2\text{Ti}_6\text{O}_{13}/\text{TiO}_2$ Heterostructure Particles, *Int. J. Photoenergy*, Hindawi 2013.

6. (2004) Synthesis and characterization of sodium titanates $\text{Na}_2\text{Ti}_3\text{O}_7$ and $\text{Na}_2\text{Ti}_6\text{O}_{13}$, *J. Solid State Chem.*, Academic Press 177, 4508–4515.
7. Tsiourvas, D., Tsetsekou, A., Arkas, M., Diplas, S., and Mastrogianni, E. (2010) Covalent attachment of a bioactive hyperbranched polymeric layer to titanium surface for the biomimetic growth of calcium phosphates, *J. Mater. Sci. Mater. Med.*, Springer 22, 85–96.
8. Vuong, N. M., Kim, D., and Kim, H. (2015) Porous Au-embedded WO_3 Nanowire Structure for Efficient Detection of CH_4 and H_2S , *Sci. Rep.* 5, 11040.
9. Adhikari, S., and Sarkar, D. (2013) Electrochemical Response for Spherical and Rod Shaped WO_3 Nanoparticles, *ISRN Nanotechnology*.
10. (2015) Characterization of $\text{Mn-Na}_2\text{WO}_4/\text{SiO}_2$ and $\text{Mn-Na}_2\text{WO}_4/\text{MgO}$ catalysts for the oxidative coupling of methane, *Appl. Catal. A*, Elsevier 497, 96–106.
11. Huang, J., Xu, X., Gu, C., Yang, M., Yang, M., and Liu, J. (2011) Large-scale synthesis of hydrated tungsten oxide 3D architectures by a simple chemical solution route and their gas-sensing properties, *J. Mater. Chem.*, The Royal Society of Chemistry 21, 13283–13289.
12. (2015) Electrochemically synthesized tungsten trioxide nanostructures for photoelectrochemical water splitting: Influence of heat treatment on physicochemical properties, photocurrent densities and electron shuttling, *Colloids Surf. A Physicochem. Eng. Asp.*, Elsevier 484, 297–303.
13. (2015) NO_2 Gas Response of WO_3 Nanofibers by Light and Thermal Activation, *Procedia Engineering*, Elsevier 120, 791–794.